symmetry

IMPACT FACTOR 2.940

CITESCORE 4.3

Article

From Five-Loop Scattering Amplitudes to Open Trees with the Loop-Tree Duality

Selomit Ramírez-Uribe, Roger José Hernández-Pinto, Germán Rodrigo and German F. R. Sborlini

MDPI

https://doi.org/10.3390/sym14122571

symmetry

MDPI

Article

From Five-Loop Scattering Amplitudes to Open Trees with the Loop-Tree Duality

Selomit Ramírez-Uribe [1,2,3], Roger José Hernández-Pinto [3,*], Germán Rodrigo [1,†] and German F. R. Sborlini [4,5]

[1] Instituto de Física Corpuscular, Universitat de València—Consejo Superior de Investigaciones Científicas, Parc Científic, E-46980 Paterna, Spain
[2] Facultad de Ciencias de la Tierra y el Espacio, Universidad Autónoma de Sinaloa, Ciudad Universitaria, Culiacán 80000, Mexico
[3] Facultad de Ciencias Físico-Matemáticas, Universidad Autónoma de Sinaloa, Ciudad Universitaria, Culiacán 80000, Mexico
[4] Departamento de Física Fundamental e IUFFyM, Universidad de Salamanca, E-37008 Salamanca, Spain
[5] Escuela de Ciencias, Ingeniería y Diseño, Universidad Europea de Valencia, Paseo de la Alameda 7, E-46010 Valencia, Spain
* Correspondence: roger@uas.edu.mx
† GR currently on leave at the European Research Council Executive Agency, European Commission, BE-1049 Brussels, Belgium. The views expressed are purely those of the writer and may not in any circumstances be regarded as stating an official position of the European Commission.

Abstract: Characterizing multiloop topologies is an important step towards developing novel methods at high perturbative orders in quantum field theory. In this article, we exploit the Loop-Tree Duality (LTD) formalism to analyse multiloop topologies that appear for the first time at five loops. Explicitly, we open the loops into connected trees and group them according to their topological properties. Then, we identify a kernel generator, the so-called N^7MLT *universal topology*, that allows us to describe any scattering amplitude of up to five loops. Furthermore, we provide factorization and recursion relations that enable us to write these multiloop topologies in terms of simpler subtopologies, including several subsets of Feynman diagrams with an arbitrary number of loops. Our approach takes advantage of many symmetries present in the graphical description of the original fundamental five-loop topologies. The results obtained in this article might shed light into a more efficient determination of higher-order corrections to the running couplings, which are crucial in the current and future precision physics program.

Keywords: perturbative QFT; higher-order calculations; multiloop Feynman integrals

Citation: Ramírez-Uribe, S.; Hernández-Pinto, R.J.; Rodrigo, G.; Sborlini, G.F.R. From Five-Loop Scattering Amplitudes to Open Trees with the Loop-Tree Duality. *Symmetry* **2022**, *14*, 2571. https://doi.org/10.3390/sym14122571

Academic Editor: Joseph L. Buchbinder

Received: 6 November 2022
Accepted: 29 November 2022
Published: 5 December 2022

1. Introduction and Motivation

Nowadays, the state-of-the-art in particle physics moves around the challenge of breaking the precision frontier. As a new generation of experiments [1–4] is approaching and current colliders are collecting enormous amounts of data; there is an increasing pressure in the theory community to provide more precise predictions. Thus, it is mandatory to explore novel techniques to deal with the complex mathematical structures behind the Standard Model (SM), and Quantum Field Theories (QFT), in general.

Most of the existing phenomenologically-relevant gauge theories, with SM and QCD as flagship examples, are not exactly solvable with our current technologies. As a consequence, we rely on approximate methods, which are valid under certain assumptions. In the high-energy limit, it turns out that the perturbation theory leads to the most reliable description of particle collisions, and provides a systematic approach to calculate precise predictions. This approach is based on series expansions involving Feynman diagrams, and reaching higher-orders requires one to computing more and more loops. At two loops and beyond [5–10], Feynman diagrams are hard to compute analytically and traditional numerical approaches quickly lose efficiency, especially when non-integrable singularities are present [11–14].

In this sense, algebraic and geometrical methods have been developed to enhance the efficiency in precision calculations, finding some competitive approaches [15–19]. Besides, several methods were proposed to include these higher-loop contributions into full cross-section calculations at higher-orders [20–54], leading to an impressive progress in precision particle physics.

Even if several strategies were devised in the last decades [55–57], the loop-calculation bottleneck is still a challenge. In this direction, the Loop-Tree Duality (LTD)[58–68] emerges as a powerful approach to transform complex loop integrals into phase-space ones, which are more suitable for numerical calculations [69–73], asymptotic expansions [74–77] and the local renormalization of ultraviolet singularities [78,79]. In particular, LTD leads to a more transparent interpretation of the singular IR-structure of multiloop integrals [59,80], paving the road for the development of novel computational strategies. For instance, LTD is a key ingredient of the so-called Four-Dimensional Unsubtraction (FDU) [79,81–83], a framework that aims to combine the real, virtual and renormalization counter-terms into a unique and integrable function in the four physical dimensions for the space-time, by-passing any additional regularization method.

Still, LTD has another interesting feature: it manifestly exhibits the causal nature of Feynman diagrams and scattering amplitudes. By using the nested residue strategy [63,84,85], one degree of freedom per loop is removed. In particular, integrating out the energy component of each loop by applying Cauchy's residue theorem, we end up with a multi-dimensional integration in an Euclidean space. This leads to an integrand representation, which is very compact and free of spurious unphysical singularities. Explicitly, adding all the terms generated by the nested residues, only those compatible with causality remain. The result is a representation that allows a direct interpretation in terms of causal entangled thresholds [63,86–90], and enables a more stable numerical calculation.

Besides, this novel LTD formulation allows a classification of the families of Feynman diagrams according to the number of sets of propagators [63]. We call Maximal Loop Topology (MLT) to those L-loop diagrams with $L+1$ sets of propagators; Next-to-Maximal Loop Topology (NMLT), if they have $L+2$ sets of propagators; and so on. Interestingly, it was proven that factorization formulae exist [84,85], and N^{k}MLT topologies can be reduced to convolutions of N^{j}MLT and MLT subtopologies (with $j < k$). Furthermore, the singular structure of the more complex topologies is constrained by these factorization properties, thus simplifying their treatment and cancellation.

The concrete purpose of this work is to study the application of the LTD approach to describe families of multiloop topologies that appear for the first time at five loops. Besides, the knowledge of the features at this topological complexity could help to improve the determination of the running couplings in gauge theories, reproducing known results up to five loops [17,91–95] and paving the road for higher-order calculations. As we did in Ref. [84], with the analysis of four-loop topologies, we define here a N^{7}MLT *universal topology* that allows one to generate the LTD representation of any possible five-loop Feynman diagram or scattering amplitude. We exploit the recursive formulation in terms of simpler subtopologies and MLT insertions, in order to extract the main features of the more complex diagrams.

The outline of this paper is the following. In Section 2, we present a brief description of the LTD framework, with special emphasis in the nested residue strategy. Then, in Section 3, we explain the construction of the *universal* N^{7}MLT kernel generator. Subtopologies counting and relevant factorization formulae are provided, and we present a concrete application example in Section 4. Finally, conclusions and possible future research directions are discussed in Section 5.

2. LTD Framework

Any loop scattering amplitude is written in the Feynman representation as an integral in the Minkowski space of the L loop momenta, $\{\ell_s\}_L$, as

$$\mathcal{A}^{(L)} = \int_{\ell_1,\ldots,\ell_L} \mathcal{A}_F^{(L)}(1,\ldots,n)\,, \tag{1}$$

where the integration measure in dimensional regularization [96–99] is given by

$$\int_{\ell_s} = -\imath\mu^{4-d} \int \frac{d^d\ell_s}{(2\pi)^d}\,, \tag{2}$$

with d the number of space-time dimensions, μ an arbitrary energy scale. The integrand in Equation (1) considers N external legs, $\{p_j\}_N$, and is composed by the product of Feynman propagators and the numerator given by the specific theory,

$$\mathcal{A}_F^{(L)}(1,\ldots,n) = \mathcal{N}(\{\ell_s\}_L,\{p_j\}_N)\, G_F(1,\ldots,n)\,, \tag{3}$$

with

$$G_F(1,\ldots,n) = \prod_{i\in 1\cup\ldots\cup n} (G_F(q_i))^{a_i}\,, \tag{4}$$

with a_i arbitrary powers. It is important to mention that in the following the powers a_i will appear only implicitly. Furthermore, the LTD expressions to be computed do not need to detail the internal configuration of each set. The Equation (4) stands for the product of Feynman propagators of one set that depends on a specific loop momentum or the union of several sets that depend on different linear combinations of the loop momenta, q_i. For instance, at one loop $q_i = \ell_1 + \sum_{j=1}^{i} p_j$, implying $q_N = \ell_1$ due to momentum conservation. We write Feynman propagators in the following alternative form,

$$G_F(q_i) = \frac{1}{(q_{i,0} - q_{i,0}^{(+)})(q_{i,0} + q_{i,0}^{(+)})}\,, \tag{5}$$

exhibiting the location of the poles, $q_{i,0}^{(+)} = \sqrt{\mathbf{q}_i^2 + m_i^2 - \imath 0}$, which includes the customary $\imath 0$ prescription of the Feynman propagators, with $q_{i,0}$ and $\mathbf{q}_i$ the temporal and spacial components of q_i, respectively, and m_i the mass of the particle. It is important to remark that the internal structure of $\mathcal{A}_F^{(L)}$ is implicitly specified via the overall tagging of the different sets of internal momenta.

To compute the LTD representation, we integrate out one of the components of the loop momenta by applying the Cauchy's residue theorem. Regarding multiloop scattering amplitudes, the LTD representation is expressed in terms of nested residues [63,85],

$$\mathcal{A}_D^{(L)}(1,\ldots,r;r+1,\ldots,n) = -2\pi\imath \sum_{i_r\in r} \mathrm{Res}(\mathcal{A}_D^{(L)}(1,\ldots,r-1;r,\ldots,n), \mathrm{Im}(\eta\cdot q_{i_r}) < 0)\,, \tag{6}$$

starting from

$$\mathcal{A}_D^{(L)}(1;2,\ldots,n) = -2\pi\imath \sum_{i_1\in 1} \mathrm{Res}(\mathcal{A}_F^{(L)}(1,\ldots,n), \mathrm{Im}(\eta\cdot q_{i_1}) < 0)\,, \tag{7}$$

where $\mathcal{A}_F^{(L)}(1,\ldots,n)$ is the integrand in the Feynman representation in Equation (1). The sets located before the semicolon have one on-shell propagator, whereas the sets appearing after the semicolon contain off-shell propagators only. The residues are evaluated through the selection of the poles with negative imaginary components by implementing

the future-like vector η selecting the component of the loop momenta to be integrated. This characteristic is taken into account by setting the condition $\mathrm{Im}(\eta \cdot q_{i_r}) < 0$, which establishes that the Cauchy contour must be always closed in the lower half plane. In this way, the interior of the contour only contains poles with a negative imaginary part. We conveniently take $\eta^\mu = (1, \mathbf{0})$, allowing it to work in the integration domain of the loop three-momenta of an Euclidean space instead of a Minkowski space.

To conclude this section, it is important to notice that LTD formalism is also useful for dealing with raised propagators or, equivalently, higher-order poles. This expressions could arise in counter-term calculations, especially beyond one loop level. In any case, it is possible to demonstrate that these amplitudes can be generated by taking derivatives, i.e.,

$$(G_F(q_i))^{\alpha_i} = \frac{1}{(\alpha_i - 1)!} \frac{\partial^{\alpha_i - 1}}{\partial \left(\left(q_{i,0}^{(+)} \right)^2 \right)^{\alpha_i - 1}} G_F(q_i) \,, \tag{8}$$

allowing us to treat them by analyzing the single-pole case. In the following, we shall present our results with $\mathcal{N}(\{\ell_s\}_L, \{p_j\}_N) = 1$, even though a realistic matrix element shall have a numerator different from unity. From the mathematical point of view, this particular scenario is the most challenging, since numerators usually reduce the complexity of the calculations. Different studies has been carried out towards these directions and can be found, for instance, in Refs. [86,100].

3. Universal Topology

In this section, we analyse the multiloop topologies that appear for the first time at five loops, i.e., the family composed by those loop topologies described by $L + 5$, $L + 6$ and $L + 7$ propagators. We start identifying the representative diagrams, followed by a unified description and the application of the LTD framework to obtain the dual opening to connected trees.

Based on the classification scheme presented in Refs. [63,85], the topological complexity of this set of diagrams corresponds to N^{7}MLT, which has $L + 5$ common sets of propagators:

$$\{1, \ldots, L+1, 12, 123, 1234, 2345\} \,, \tag{9}$$

and two additional specific sets distinguishing them from each other. To achieve a global representation of this family, we first need to unravel the representative topologies through the identification of the distinctive pair of sets.

Inspired by the N^{4}MLT *universal topology* [84], we recall the concept of a current to encode in a compact form the distinctive sets. This arrangement is diagrammatically represented in Figure 1. Each specific topology is characterized by a pair of sets from the list $\{23, 24, 25, 34, 35, 45, 234, 235, 245, 34\}$. It is important to take into account that one of the internal sets, 2345, is imposed by momentum conservation. The total number of distinctive pairs is fifteen, and they can be conveniently grouped in five channels, as presented in Table 1 and displayed in Figure 2. Many nonplanar topologies arise; in fact, they account for ten from the total of fifteen.

Each pair of sets from Table 1 is associated to a single Feynman diagram. The first L common sets of propagators depend on one characteristic loop momentum ℓ_s, and the momenta of their propagators have the form

$$q_{i_s} = \ell_s + k_{i_s} \qquad s \in \{1, \ldots, L\} \,. \tag{10}$$

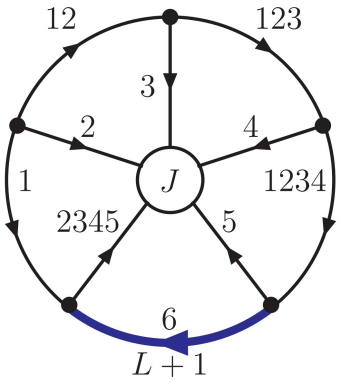

Figure 1. Diagrammatic representation of the general N^{7}MLT topology. The current J considers all the possible combinations among the internal propagators. The blue line merges $L-4$ propagators, which encodes a MLT with $L-5$ loops and $L-4$ propagators introduced in Ref. [63].

The remaining five common sets are denoted as linear combinations of all the loop momenta, explicitly:

$$\begin{aligned} q_{i_{(L+1)}} &= -\sum_{s=1}^{L} \ell_s + k_{i_{(L+1)}}\,, \quad q_{i_{12}} = -\ell_1 - \ell_2 + k_{i_{12}}\,, \\ q_{i_{123}} &= -\sum_{s=1}^{3} \ell_s + k_{i_{123}}\,, \quad q_{i_{1234}} = -\sum_{s=1}^{4} \ell_s + k_{i_{1234}}\,, \\ q_{i_{2345}} &= -\sum_{s=2}^{5} \ell_s + k_{i_{2345}}\,, \end{aligned} \tag{11}$$

with $k_{i_s}, k_{i_{(L+1)}}, k_{i_{12}}, k_{i_{123}}, k_{i_{1234}}$ and $k_{i_{2345}}$ linear combinations of external momenta.

Table 1. Pair of sets identifying the representative topologies of the N^{7}MLT family. The star indicates that the set is associated to a nonplanar diagram.

J_1:	$\{234,23\}$	$\{234,24\}$ $\star$	$\{234,34\}$
J_2:	$\{235,23\}$ $\star$	$\{235,25\}$ $\star$	$\{235,35\}$ $\star$
J_3:	$\{245,24\}$ $\star$	$\{245,25\}$ $\star$	$\{245,45\}$ $\star$
J_4:	$\{345,34\}$	$\{345,35\}$ $\star$	$\{345,45\}$
J_5:	$\{23,45\}$	$\{24,35\}$ $\star$	$\{25,34\}$ $\star$

The extra sets are the distinctive key to generate each of the fifteen topologies. We identify the momenta of their propagators as different linear combinations of ℓ_2, ℓ_3, ℓ_4 and ℓ_5, writing them as

$$q_{i_{rs}} = -\ell_r - \ell_s + k_{i_{rs}}\,, \quad q_{i_{rst}} = -\ell_r - \ell_s - \ell_t + k_{i_{rst}}\,, \qquad r,s \in \{2,3,4,5\}\,. \tag{12}$$

In order to achieve a single expression to represent the N^{7}MLT topologies, we merge the sets presented in Table 1 into a current labeled as J,

$$J = \cup_{i=1}^{5} J_i\,. \tag{13}$$

The setting of this scenario allows us to assemble the Feynman representation of the N^{7}MLT family as

$$\mathcal{A}^{(L)}_{\mathrm{N^7MLT}} = \int_{\ell_1,\ldots,\ell_L} \mathcal{A}^{(L)}_{F}(1,\ldots,L+1,12,123,1234,2345,J)\,, \tag{14}$$

diagrammatic, represented in accordance with Figure 1.

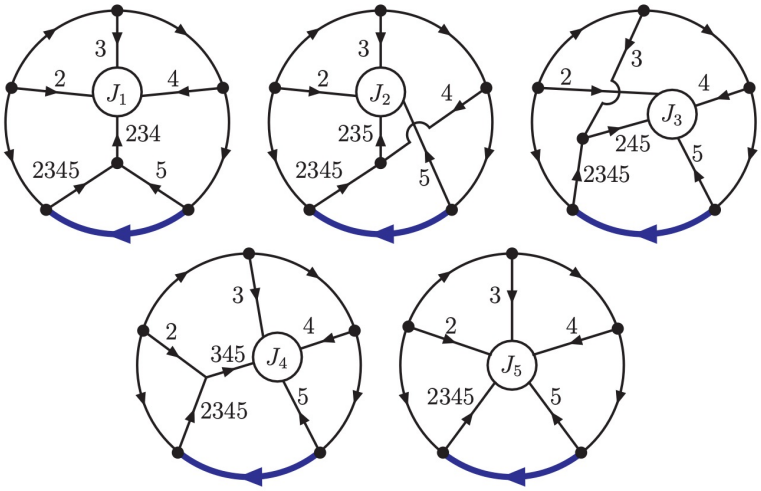

Figure 2. Diagrammatic representation of the multiloop topologies associated to the sets defined in Table 1, where only the internal propagators are labeled. The blue bold line represents an arbitrary number of propagators. In the case of the channel J_5, the characterize sets are established by merging two of the common sets, as depicted in Figure 3.

The dual opening of Equation (14) is computed by the direct application of the nested residues through the LTD framework. With the purpose of obtaining a manageable dual expression, we also propose an ansatz based in a graphical interpretation of the opening. The comparison between these two ingredients allow us to achieve a LTD representation exhibited in a factorized form in terms of simpler subtopologies,

$$\begin{aligned}
&\mathcal{A}^{(L)}_{\mathrm{N^7MLT}}(1,\ldots,L+1,12,123,1234,2345,J)\\
&=\mathcal{A}^{(5)}_{\mathrm{N^6MLT}}(1,\ldots,5,12,123,1234,2345,J)\otimes\mathcal{A}^{(L-5)}_{\mathrm{MLT}}(6,\ldots,L+1)\\
&+\mathcal{A}^{(4)}_{\mathrm{N^5MLT}}(1\cup 2345,2,3,4,5\cup 1234,12,123,J)\otimes\mathcal{A}^{(L-4)}_{\mathrm{MLT}}(\overline{6},\ldots,\overline{L+1})\,,
\end{aligned}\tag{15}$$

where the bar in a set means that the momentum flows of the set are reversed. The term $\mathcal{A}^{(L)}_{\mathrm{N^{k-1}MLT}}$ refers to the integrand of the corresponding topology in the LTD representation; integration over the L loop momenta is assumed. The convolution symbol indicates that each component is open independently, while the on-shell conditions of all elements act together over the remaining off-shell propagators. Regarding the selected on-shell propagators, they are restricted so as not to generate disjoint trees due to the dual opening.

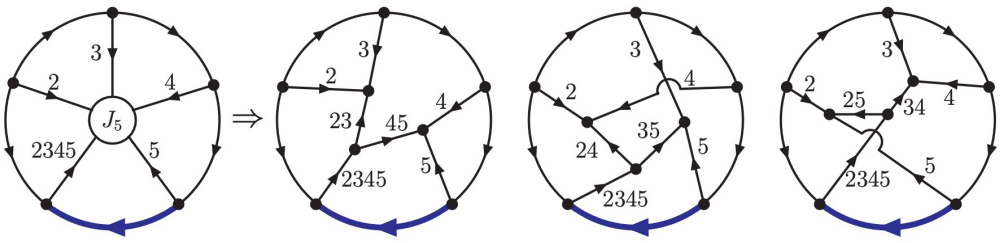

Figure 3. Diagrammatic representation of the multiloop topologies conforming the channel J_5.

The LTD expression in Equation (15) opens any multiloop N^{7}MLT topology to connected trees, furthermore, it is valid for all N^{k-1}MLT configurations with $k \leq 7$. The dual opening interpretation is depicted in Figure 4, where the diagram associated to the term $\mathcal{A}^{(5)}_{\mathrm{N^6MLT}}$ on the r.h.s. of Equation (15) contemplate all possible configurations with five on-shell propagators in the sets $\{1,2,3,4,12,123,1234,2345,J\}$, and the contribution of $\mathcal{A}^{(4)}_{\mathrm{N^5MLT}}$ in the second term assumes four on-shell conditions selected from

$\{1 \cup 2345, 2, 3, 4, 5 \cup 1234, 12, 123, J\}$. The term $\mathcal{A}^{(L-5)}_{\text{MLT}}(6, \ldots, L+1)$ is opened according to the MLT opening introduced in Ref. [63]; in $\mathcal{A}^{(L-4)}_{\text{MLT}}(\overline{6}, \ldots, \overline{L+1})$ all the momentum flows are reversed and all the sets contain one on-shell propagator.

The unfolding of Equation (15) is computed recursively through the subtopologies arising, for instance, the five-loop contribution opens as follows

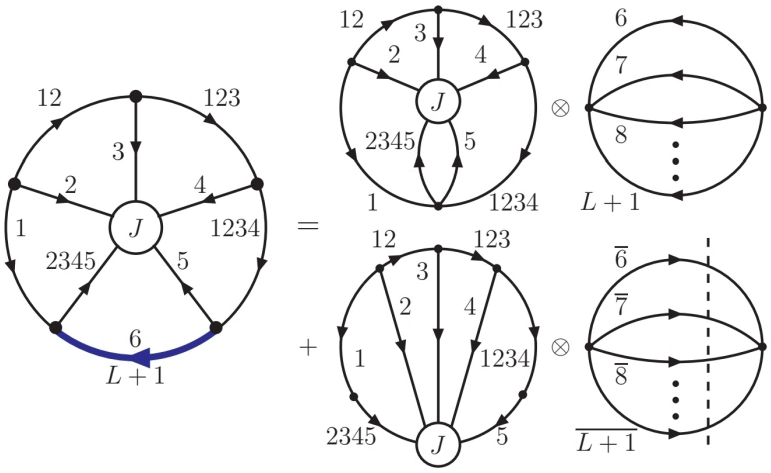

Figure 4. Diagrammatic representation for the factorized opening of the multiloop N^{7}MLT general topology, described by Equation (15). Only the on-shell cut of the last MLT-like subtopology with reversed momentum flow is shown.

$$\begin{aligned}
&\mathcal{A}^{(5)}_{\text{N}^6\text{MLT}}(1, \ldots, 5, 12, 123, 1234, 2345, J) \\
&= \mathcal{A}^{(5)}_{\text{N}^4\text{MLT}}(1, \ldots, 5, 12, 123, 1234, 2345) \\
&+ \sum_{s \in J} \mathcal{A}^{(4)}_{\text{N}^4\text{MLT}}(1, \ldots, 5, 12, 123, 1234, 2345, \mathbf{s}) \, .
\end{aligned} \tag{16}$$

The first term in the r.h.s. gives a LTD contribution with all the propagators with momenta in J remaining off shell. The second term on the r.h.s. of Equation (16) considers all the contributions with a pair of propagators with momenta belonging to Table 1, therefore, these dual trees correspond to a single representative channel. The bold symbol, $\mathbf{s}$, is used to identify the contributions with on-shell propagators belonging to J.

Concerning the four-loop subtopology in Equation (15), the dual opening is given by

$$\begin{aligned}
&\mathcal{A}^{(4)}_{\text{N}^5\text{MLT}}(1 \cup 2345, 2, 3, 4, 5 \cup 1234, 12, 123, J) \\
&= \mathcal{A}^{(4)}_{\text{N}^3\text{MLT}}(1 \cup 2345, 2, 3, 4, 5 \cup 1234, 12, 123) \\
&+ \sum_{s \in J} \mathcal{A}^{(3)}_{\text{N}^3\text{MLT}}(1 \cup 2345, 2, 3, 4, 5 \cup 1234, 12, 123, \mathbf{s}) \, ,
\end{aligned} \tag{17}$$

where similar to Equation (16), the first term in the r.h.s. considers all the pair of propagators with momenta in J off shell, whereas the second term is associated to a specific three-loop N^{3}MLT topology.

Every representative topology in the N^{7}MLT family have common dual terms, those associated to the first term in the r.h.s. in Equations (16) and (17), respectively,

$$\mathcal{A}^{(5)}_{\text{N}^4\text{MLT}}(1, \ldots, 5, 12, 123, 1234, 2345) \quad \text{and} \quad \mathcal{A}^{(4)}_{\text{N}^3\text{MLT}}(1 \cup 2345, 2, 3, 4, 5 \cup 1234, 12, 123) \, . \tag{18}$$

These contributions can be graphical represented with the first diagram in the r.h.s. of both sums depicted in Figure 4 by replacing J with a five point interaction among the internal sets, i.e., by taking J as an empty set. To entirely unfold them and obtain the explicit dual terms, we continue to open the subtopologies recursively. Even if the ordering of opening

any topology is arbitrary, following the guide of a diagrammatic interpretation allows us to work in a more manageable form.

Concerning the common dual terms in the N^{7}MLT topologies, we have that

$$\mathcal{A}^{(4)}_{\mathrm{N^3MLT}}(1\cup 2345,2,3,4,5\cup 1234,12,123) \tag{19}$$

opens according Ref. [84] by considering the set 234 as empty and, in the case of the five-loop contribution, the explicit dual opening is given by

$$\begin{aligned}
&\mathcal{A}^{(5)}_{\mathrm{N^4MLT}}(1,\ldots,5,12,123,1234,2345)\\
=&\mathcal{A}^{(4)}_{\mathrm{N^4MLT}}(1,2,3,4,12,123,1234)\otimes\mathcal{A}^{(1)}_{\mathrm{MLT}}(5,2345)\\
&+\Big[\mathcal{A}^{(3)}_{\mathrm{NMLT}}(1,2,3,12,123)+\Big(\mathcal{A}^{(2)}_{\mathrm{MLT}}(1,2,12)+\mathcal{A}^{(2)}_{\mathrm{MLT}}(1,\bar{3})\Big)\\
&\otimes\mathcal{A}^{(1)}_{\mathrm{MLT}}(\bar{4})\Big]\otimes\mathcal{A}^{(2)}_{\mathrm{MLT}}(\bar{5},\overline{2345})+\Big[\mathcal{A}^{(2)}_{\mathrm{MLT}}(\overline{1234},2\cup\overline{12})\otimes\mathcal{A}^{(1)}_{\mathrm{MLT}}(3,123)\\
&+\mathcal{A}^{(3)}_{\mathrm{MLT}}(\overline{1234},\bar{3},\overline{123})+\mathcal{A}^{(2)}_{\mathrm{MLT}}(\overline{1234},2\cup\overline{312})\otimes\mathcal{A}^{(1)}_{\mathrm{MLT}}(\bar{4})\\
&+\Big(\mathcal{A}^{(2)}_{\mathrm{MLT}}(3,\overline{12})+\mathcal{A}^{(2)}_{\mathrm{MLT}}(\overline{1234},2\cup\bar{3}\cup\overline{12})\Big)\otimes\mathcal{A}^{(1)}_{\mathrm{MLT}}(4)\Big]\otimes\mathcal{A}^{(2)}_{\mathrm{MLT}}(5,2345)\,.
\end{aligned} \tag{20}$$

The expression given in Equation (20) is understood in the same way as in Ref. [63], where the convolution means that we must combine the opening of one subset of momenta with the opening of other subset. For instance at three-loops, inside $\mathcal{A}^{(3)}_{\mathrm{NMLT}}(1,2,3,4,12)$, we have the contribution

$$\begin{aligned}
&\mathcal{A}^{(2)}_{\mathrm{MLT}}(1,2,12)\otimes\mathcal{A}^{(1)}_{\mathrm{MLT}}(3,4)\\
&=\int_{\ell_1,\ell_2,\ell_3}\Big[\mathcal{A}^{(3)}_{D}(\bar{2},\overline{12},\bar{4};1,3)+\mathcal{A}^{(3)}_{D}(1,\overline{12},\bar{4};2,3)+\mathcal{A}^{(3)}_{D}(1,2,\bar{4};12,3)+(\bar{4}\leftrightarrow 3)\Big]\,,
\end{aligned} \tag{21}$$

where $\mathcal{A}^{(L)}_{\mathrm{MLT}}(1,\ldots,12)$ is defined as

$$\mathcal{A}^{(L)}_{\mathrm{MLT}}(1,\ldots,n)=\int_{\ell_1,\ldots,\ell_L}\sum_{i=1}^{n}\mathcal{A}^{(L)}_{D}(1,\ldots,i-1,\overline{i+1},\ldots,\overline{n};i)\,. \tag{22}$$

It is important to notice from this simple example that in order to write effortless expressions, the result of simpler topologies must be known. For five-loop topologies, the definitions presented in Refs. [63,84] must be taken into account. Hence, the number of dual terms arising from the contributions in Equations (19) and (20) for an arbitrary number of loops is given by $11(6L-19)$.

The contributions corresponding to the second term in the r.h.s. in Equations (16) and (17) depend on the particular topology to be opened. In the following section, we take a specific example and present the explicit contributions characterising the topology.

4. Specific Channels

In order to deepen in the dual opening methodology, we present the development of the topology associated to the pair of sets $\{234,23\}$ belonging to the current J_1. The factorized dual opening is obtained through the application of Equation (15) replacing J by $\{234,23\}$. The diagrammatic representation of the associated topology, and its factorized dual opening is depicted in Figure 5.

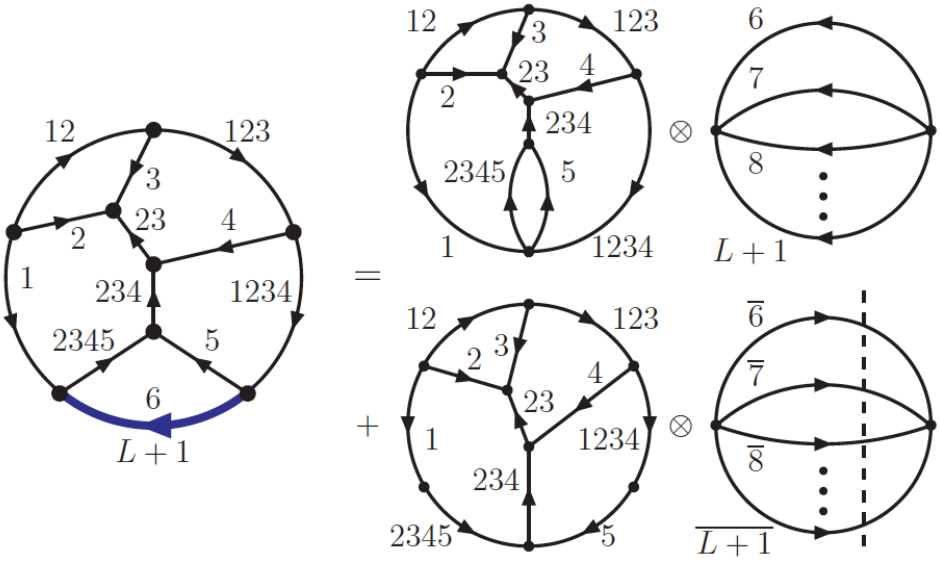

Figure 5. Diagrammatic representation for the topology having $J = \{234, 23\}$ and its factorized dual opening from Equation (15).

The common terms in the fifteen topologies are the ones associated to Equations (19) and (20), which are illustrated with the first diagram in the r.h.s. of each sum in Figure 6. From the previous section, we know that the contributions for this specific topology arise from the second term in the r.h.s. of Equations (16) and (17), which are diagrammatically represented by the sum of the second and third diagrams in the r.h.s. of each sum in Figure 6.

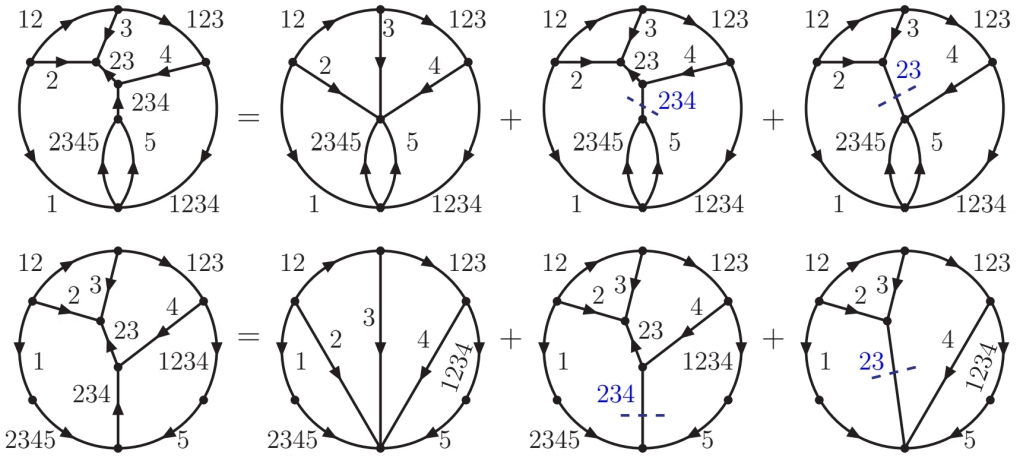

Figure 6. Diagrammatic representation of the dual opening of the contributions associated to the five-loop N^{4}MLT in Equation (20) (**top**) and the four-loop N^{3}MLT in Equation (19) (**bottom**).

The unfolding of the second term in the r.h.s. of Equation (16) with $s \in \{234, 23\}$ is given by

$$
\begin{aligned}
&\mathcal{A}^{(4)}_{\mathrm{N^4MLT}}(1,\ldots,5,12,123,1234,2345,23,234)\\
&+\mathcal{A}^{(4)}_{\mathrm{N^4MLT}}(1,\ldots,5,12,123,1234,2345,23)\\
=&\Big[\Big(\mathcal{A}^{(3)}_{\mathrm{N^2MLT}}(1,2,3,12,123,23)+\mathcal{A}^{(2)}_{\mathrm{MLT}}(1,2,12)\otimes\mathcal{A}^{(1)}_{\mathrm{MLT}}(\overline{4})+\mathcal{A}^{(3)}_{\mathrm{MLT}}(1,\overline{3},\overline{4})\Big)\\
&\otimes\mathcal{A}^{(1)}_{D}(\overline{234})+\Big(\mathcal{A}^{(2)}_{\mathrm{MLT}}(\overline{1234},2\cup\overline{12})\otimes\mathcal{A}^{(1)}_{\mathrm{MLT}}(3,4\cup23)+\mathcal{A}^{(3)}_{\mathrm{MLT}}(\overline{1234},\overline{3},\overline{4}\cup\overline{23})\\
&+\mathcal{A}^{(3)}_{\mathrm{MLT}}(12,3,4)+\mathcal{A}^{(3)}_{\mathrm{MLT}}(4\cup\overline{1234},2\cup\overline{3}\cup\overline{12},\overline{123})\Big)\otimes\mathcal{A}^{(1)}_{D}(234)\Big]\otimes\mathcal{A}^{(1)}_{\mathrm{MLT}}(5,2345)\\
+&\Big[\Big(\mathcal{A}^{(2)}_{\mathrm{MLT}}(1,2,12)+\mathcal{A}^{(2)}_{\mathrm{MLT}}(1,\overline{3})\Big)\otimes\Big(\mathcal{A}^{(2)}_{\mathrm{MLT}}(4,5,2345)+\mathcal{A}^{(1)}_{\mathrm{MLT}}(5,2345)\otimes\mathcal{A}^{(1)}_{\mathrm{MLT}}(\overline{1234})\Big)\\
&+\mathcal{A}^{(1)}_{\mathrm{MLT}}(2\cup\overline{3},12)\otimes\mathcal{A}^{(2)}_{\mathrm{MLT}}(5,2345)\otimes\mathcal{A}^{(1)}_{\mathrm{MLT}}(\overline{1234})\Big]\otimes\mathcal{A}^{(1)}_{D}(\overline{23})\\
+&\Big[\Big(\mathcal{A}^{(2)}_{\mathrm{MLT}}(\overline{123},\overline{3},12)+\mathcal{A}^{(2)}_{\mathrm{MLT}}(\overline{123},2)\Big)\otimes\mathcal{A}^{(2)}_{\mathrm{MLT}}(4,5,2345)+\Big(\mathcal{A}^{(2)}_{\mathrm{MLT}}(\overline{4}\cup\overline{123},\overline{3},12)\\
&+\mathcal{A}^{(2)}_{\mathrm{MLT}}(\overline{4}\cup\overline{123},2)\Big)\otimes\mathcal{A}^{(1)}_{\mathrm{MLT}}(5,2345)\otimes\mathcal{A}^{(1)}_{\mathrm{MLT}}(\overline{1234})\Big]\otimes\mathcal{A}^{(1)}_{D}(23)\,,
\end{aligned}
\tag{23}
$$

and the one corresponding to Equation (17),

$$
\begin{aligned}
&\mathcal{A}^{(3)}_{\mathrm{N^3MLT}}(1\cup2345,2,3,4,5\cup1234,12,123,23,234)\\
&+\mathcal{A}^{(3)}_{\mathrm{N^3MLT}}(1\cup2345,2,3,4,5\cup1234,12,123,23)\\
&=\Big[\mathcal{A}^{(3)}_{\mathrm{N^2MLT}}(1\cup2345,2,3,12,123,23)+\mathcal{A}^{(2)}_{\mathrm{MLT}}(1\cup2345,2,12)\otimes\mathcal{A}^{(1)}_{\mathrm{MLT}}(\overline{4})\\
&+\mathcal{A}^{(3)}_{\mathrm{MLT}}(1\cup2345,\overline{3},\overline{4})\Big]\otimes\mathcal{A}^{(1)}_{D}(\overline{234})\\
&+\Big[\mathcal{A}^{(2)}_{\mathrm{MLT}}(\overline{5}\cup\overline{1234},2\cup\overline{12})\otimes\mathcal{A}^{(1)}_{\mathrm{MLT}}(3,4\cup23)+\mathcal{A}^{(3)}_{\mathrm{MLT}}(\overline{5}\cup\overline{1234},\overline{3},\overline{4}\cup\overline{23})\\
&+\mathcal{A}^{(3)}_{\mathrm{MLT}}(\overline{12},3,4)+\mathcal{A}^{(3)}_{\mathrm{MLT}}(\overline{5}\cup\overline{1234}\cup\overline{4},2\cup\overline{3}\cup\overline{12},\overline{123})\Big]\otimes\mathcal{A}^{(1)}_{D}(234)\\
&+\Big(\mathcal{A}^{(2)}_{\mathrm{MLT}}(1\cup2345,2,12)+\mathcal{A}^{(2)}_{\mathrm{MLT}}(1\cup2345,\overline{3})\Big)\otimes\mathcal{A}^{(1)}_{\mathrm{MLT}}(4,5\cup1234)\otimes\mathcal{A}^{(1)}_{D}(\overline{23})\\
&+\Big[\Big(\mathcal{A}^{(2)}_{\mathrm{MLT}}(\overline{123},\overline{3},12)+\mathcal{A}^{(2)}_{\mathrm{MLT}}(\overline{123},2)\Big)\otimes\mathcal{A}^{(1)}_{\mathrm{MLT}}(4,5\cup1234)\\
&+\mathcal{A}^{(1)}_{\mathrm{MLT}}(2\cup\overline{3},12)\otimes\mathcal{A}^{(2)}_{\mathrm{MLT}}(\overline{4},\overline{5}\cup\overline{1234})\Big]\otimes\mathcal{A}^{(1)}_{D}(23)\,.
\end{aligned}
\tag{24}
$$

The sets in blue in the arguments of the terms in the l.h.s. of Equations (23) and (24) indicate the set that we use as a starting cut in the second and third diagram of each sum in Figure 6. After this action, we end up with known subtopologies that we recursively compute by applying the results from Refs. [63,84]. The total number of dual terms emerging from Equations (23) and (24) for an arbitrary number of loops is given by $119L-380$. The number of dual terms arising from every specific channel for an arbitrary number of loops is summarized in Table 2.

Table 2. Numbers of dual terms for the individual channels. The blue star denotes all non-equivalent configurations. The remaining possibilities can be obtained from the ones with the blue star.

J_1:		$\{234,23\}$	$119\,L-380$	$\star$	$\{234,24\}$	$132\,L-418$	$\{234,34\}$	$119\,L-380$
J_2:	$\star$	$\{235,23\}$	$143\,L-473$	$\star$	$\{235,25\}$	$158\,L-519$	$\star$ $\{235,35\}$	$165\,L-554$
J_3:	$\star$	$\{245,24\}$	$165\,L-554$	$\star$	$\{245,25\}$	$165\,L-554$	$\star$ $\{245,45\}$	$165\,L-583$
J_4:		$\{345,34\}$	$143\,L-500$	$\star$	$\{345,35\}$	$165\,L-583$	$\{345,45\}$	$158\,L-575$
J_5:		$\{23,45\}$	$143\,L-500$	$\star$	$\{24,35\}$	$165\,L-554$	$\star$ $\{25,34\}$	$143\,L-473$

It is worth mentioning that among the fifteen configurations, some of them are topologically equivalent. For example, the dual representation of the diagram characterized by $\{234,34\}$ can be obtained from the dual representation computed to the topology characterized with $\{234,23\}$, by the substitution $23\to34$ and the exchange $2\leftrightarrow4$,

$$\mathcal{A}^{(L)}_{\mathrm{N^7MLT}}(1,\ldots,234,23) \xrightarrow[2\leftrightarrow 4]{23\to 34} \mathcal{A}^{(L)}_{\mathrm{N^7MLT}}(1,\ldots,234,34)\,.$$

For the remaining equivalent topologies, we require to exchange $2 \leftrightarrow 4$ and $5 \leftrightarrow 2345$, as well as applying the proper substitution between the distinctive sets. Explicitly, we have that

$$\begin{aligned}
&\mathcal{A}^{(L)}_{\mathrm{N^7MLT}}(1,\ldots,235,23) \xrightarrow[2\leftrightarrow 4,\ 5\leftrightarrow 2345]{235\to 25,\ 23\to 34} \mathcal{A}^{(L)}_{\mathrm{N^7MLT}}(1,\ldots,25,34)\,,\\
&\mathcal{A}^{(L)}_{\mathrm{N^7MLT}}(1,\ldots,235,35) \xrightarrow[2\leftrightarrow 4,\ 5\leftrightarrow 2345]{235\to 25,\ 35\to 245} \mathcal{A}^{(L)}_{\mathrm{N^7MLT}}(1,\ldots,245,25)\,,\\
&\mathcal{A}^{(L)}_{\mathrm{N^7MLT}}(1,\ldots,245,24) \xrightarrow[2\leftrightarrow 4,\ 5\leftrightarrow 2345]{245\to 35} \mathcal{A}^{(L)}_{\mathrm{N^7MLT}}(1,\ldots,24,35)\,,\\
&\mathcal{A}^{(L)}_{\mathrm{N^7MLT}}(1,\ldots,245,45) \xrightarrow[2\leftrightarrow 4,\ 5\leftrightarrow 2345]{245\to 35,\ 45\to 345} \mathcal{A}^{(L)}_{\mathrm{N^7MLT}}(1,\ldots,345,35)\,,\\
&\mathcal{A}^{(L)}_{\mathrm{N^7MLT}}(1,\ldots,345,34) \xrightarrow[2\leftrightarrow 4,\ 5\leftrightarrow 2345]{345\to 45,\ 34\to 23} \mathcal{A}^{(L)}_{\mathrm{N^7MLT}}(1,\ldots,23,45)\,.
\end{aligned}$$

Certainly, there are topologies that cannot be obtained from a direct replacement of indices, mainly those related with non planar topologies. Nevertheless, the direct application of the LTD shows that there are no disjoint trees in the forest of the N^{7}MLT topology and these feature is important to compute physical observables at high precision. Therefore, we let the application of these expressions go to further analysis.

5. Conclusions and Outlook

In this work, we applied the Loop-Tree Duality (LTD) and the nested residue representation to characterize all the possible five-loop Feynman diagrams. Following the approach presented in Ref. [84], we identified a *universal topology*, i.e., the N^{7}MLT diagram, and then related the possible subtopologies through factorization formulae. As already known for simpler cases (such as N^{4}MLT, N^{3}MLT and N^{2}MLT, studied in Refs. [63,84,86]), these factorization formulae lead to a recursive representation of complex topologies in terms of simpler ones. In this way, it is possible to understand the singular properties of all the five-loop amplitudes in terms of objects with a lower complexity.

Beyond the important recursive relations found among multiloop amplitudes, the developments shown in this paper could be further explored to simplify the calculation of important quantities at five-loop accuracy. In this way, the LTD representation and its factorization properties could allow us to break the bottleneck of multiloop multileg calculations in QFT.

Author Contributions: All authors contributed equally to this work. S.R.-U. was in charge of doing the diagrams and formatting the manuscript. All authors have read and agreed to the published version of the manuscript.

Funding: This research was partially funded by MCIN/AEI/10.13039/501100011033, Grant No. PID2020-114473GB-I00, Consejo Nacional de Ciencia y Tecnología and Universidad Autónoma de Sinaloa, CONACyT (México) Project No. 320856 (Paradigmas y Controversias de la Ciencia 2022), Ciencia de Frontera 2021-2042, Sistema Nacional de Investigadores, PROFAPI 2022 Grant No. PRO_A1_024 (Universidad Autónoma de Sinaloa), Programas Propios II (Universidad de Salamanca), EU Horizon 2020 research and innovation program STRONG-2020 project under grant agreement No. 824093 and MSCA H2020 USAL4EXCELLENCE-PROOPI-391 cofund project under grant agreement No. 101034371.

Data Availability Statement: Not applicable.

Conflicts of Interest: The authors declare no conflict of interest.

References

1. Abada, A.; Abbrescia, M.; AbdusSalam, S.S.; Abdyukhanov, I.; Abelleira Fernandez, J.; Abramov, A.; Aburaia, M.; Acar, A.O.; Adzic, P.R.; Agrawal, P.; et al. FCC Physics Opportunities: Future Circular Collider Conceptual Design Report Volume 1. *Eur. Phys. J. C* **2019**, *79*, 474. [CrossRef]
2. Bambade, P.; Barklow, T.; Behnke, T.; Berggren, M.; Brau, J.; Burrows, P.; Denisov, D.; Faus-Golfe, A.; Foster, B.; Fujii, K.; et al. The International Linear Collider: A Global Project. *arXiv* **2019**, arXiv:1903.01629.
3. Roloff, P.; de Blas, J.; Franceschini, R.; Riva, F.; Schnoor, U.; Spannoswsky, M.; Wells, J.D.; Wulzer, A.; Zupan, J.; Alipour-Fard, S.; et al. The Compact Linear e^+e^- Collider (CLIC): Physics Potential. *arXiv* **2018**, arXiv:1812.07986.
4. CEPC Study Group. CEPC Conceptual Design Report: Volume 2-Physics & Detector. *arXiv* **2018**, arXiv:1811.10545.
5. Gehrmann, T.; Kara, D. The $Hb\bar{b}$ form factor to three loops in QCD. *JHEP* **2014**, *9*, 174.
6. Broggio, A.; Gnendiger, C.; Signer, A.; Stöckinger, D.; Visconti, A. Computation of $H \to gg$ in $DRED$ and FDH: Renormalization, operator mixing, and explicit two-loop results. *Eur. Phys. J. C* **2015**, *75*, 418.
7. Page, B.; Pittau, R. Two-loop off-shell QCD amplitudes in FDR. *JHEP* **2015**, *11*, 183.
8. Cacciari, M.; Dreyer, F.A.; Karlberg, A.; Salam, G.P.; Zanderighi, G. Fully Differential Vector-Boson-Fusion Higgs Production at Next-to-Next-to-Leading Order. *Phys. Rev. Lett.* **2015**, *115*, 082002, Erratum in *Phys. Rev. Lett.* **2018**, *120*, 139901. [CrossRef]
9. Aybat, S.M.; Dixon, L.J.; Sterman, G.F. The Two-loop anomalous dimension matrix for soft gluon exchange. *Phys. Rev. Lett.* **2006**, *97*, 072001.
10. Dreyer, F.A.; Karlberg, A. Vector-Boson Fusion Higgs Production at Three Loops in QCD. *Phys. Rev. Lett.* **2016**, *117*, 072001.
11. Catani, S. The Singular behavior of QCD amplitudes at two loop order. *Phys. Lett. B* **1998**, *427*, 161–171. [CrossRef]
12. Bern, Z.; Del Duca, V.; Kilgore, W.B.; Schmidt, C.R. The infrared behavior of one loop QCD amplitudes at next-to-next-to leading order. *Phys. Rev. D* **1999**, *60*, 116001.
13. Becher, T.; Neubert, M. Infrared singularities of scattering amplitudes in perturbative QCD. *Phys. Rev. Lett.* **2009**, *102*, 162001, Erratum in *Phys. Rev. Lett.* **2013**, *111*, 199905. [CrossRef]
14. Gehrmann-De Ridder, A.; Gehrmann, T.; Glover, E.W.N.; Heinrich, G. Infrared structure of e+ e- —> 3 jets at NNLO. *JHEP* **2007**, *11*, 58.
15. Bhattacharya, A.; Moult, I.; Stewart, I.W.; Vita, G. Helicity Methods for High Multiplicity Subleading Soft and Collinear Limits. *JHEP* **2019**, *5*, 192.
16. Borinsky, M. Tropical Monte Carlo quadrature for Feynman integrals. *arXiv* **2020**, arXiv:2008.12310.
17. Chetyrkin, K.G.; Tkachov, F.V. Integration by Parts: The Algorithm to Calculate beta Functions in 4 Loops. *Nucl. Phys.* **1981**, *B192*, 159–204. [CrossRef]
18. Laporta, S. High precision calculation of multiloop Feynman integrals by difference equations. *Int. J. Mod. Phys. A* **2000**, *15*, 5087–5159.
19. Herzog, F. Geometric IR subtraction for final state real radiation. *JHEP* **2018**, *8*, 6.
20. Catani, S.; Seymour, M. The Dipole formalism for the calculation of QCD jet cross-sections at next-to-leading order. *Phys.Lett.* **1996**, *B378*, 287–301.
21. Catani, S.; Seymour, M. A General algorithm for calculating jet cross-sections in NLO QCD. *Nucl. Phys.* **1997**, *B485*, 291–419. [CrossRef]
22. Catani, S.; Grazzini, M. Infrared factorization of tree level QCD amplitudes at the next-to-next-to-leading order and beyond. *Nucl. Phys. B* **2000**, *570*, 287–325.
23. de Florian, D.; Grazzini, M. Next-to-next-to-leading logarithmic corrections at small transverse momentum in hadronic collisions. *Phys. Rev. Lett.* **2000**, *85*, 4678–4681.
24. Catani, S.; Dittmaier, S.; Seymour, M.H.; Trocsanyi, Z. The Dipole formalism for next-to-leading order QCD calculations with massive partons. *Nucl.Phys.* **2002**, *B627*, 189–265.
25. Frixione, S.; Kunszt, Z.; Signer, A. Three jet cross-sections to next-to-leading order. *Nucl. Phys.* **1996**, *B467*, 399–442.
26. Frixione, S. A General approach to jet cross-sections in QCD. *Nucl. Phys. B* **1997**, *507*, 295–314.
27. Frixione, S.; Grazzini, M. Subtraction at NNLO. *JHEP* **2005**, *6*, 10.
28. Bozzi, G.; Catani, S.; de Florian, D.; Grazzini, M. The q(T) spectrum of the Higgs boson at the LHC in QCD perturbation theory. *Phys. Lett. B* **2003**, *564*, 65–72.
29. Bozzi, G.; Catani, S.; de Florian, D.; Grazzini, M. Transverse-momentum resummation and the spectrum of the Higgs boson at the LHC. *Nucl. Phys. B* **2006**, *737*, 73–120.
30. Catani, S.; Grazzini, M. An NNLO subtraction formalism in hadron collisions and its application to Higgs boson production at the LHC. *Phys. Rev. Lett.* **2007**, *98*, 222002.
31. Catani, S.; Grazzini, M. QCD transverse-momentum resummation in gluon fusion processes. *Nucl. Phys. B* **2011**, *845*, 297–323.
32. Catani, S.; Cieri, L.; de Florian, D.; Ferrera, G.; Grazzini, M. Vector boson production at hadron colliders: Hard-collinear coefficients at the NNLO. *Eur. Phys. J. C* **2012**, *72*, 2195.
33. Catani, S.; Cieri, L.; de Florian, D.; Ferrera, G.; Grazzini, M. Universality of transverse-momentum resummation and hard factors at the NNLO. *Nucl. Phys. B* **2014**, *881*, 414–443.
34. Bonciani, R.; Catani, S.; Grazzini, M.; Sargsyan, H.; Torre, A. The q_T subtraction method for top quark production at hadron colliders. *Eur. Phys. J. C* **2015**, *75*, 581.

35. Cieri, L.; Chen, X.; Gehrmann, T.; Glover, E.W.N.; Huss, A. Higgs boson production at the LHC using the q_T subtraction formalism at N^{3}LO QCD. *JHEP* **2019**, *2*, 96.
36. Catani, S.; Devoto, S.; Grazzini, M.; Kallweit, S.; Mazzitelli, J.; Sargsyan, H. Top-quark pair hadroproduction at next-to-next-to-leading order in QCD. *Phys. Rev. D* **2019**, *99*, 051501.
37. Buonocore, L.; Grazzini, M.; Tramontano, F. The q_T subtraction method: Electroweak corrections and power suppressed contributions. *Eur. Phys. J. C* **2020**, *80*, 254.
38. Kosower, D.A. Antenna factorization of gauge theory amplitudes. *Phys. Rev. D* **1998**, *57*, 5410–5416. [CrossRef]
39. Campbell, J.M.; Glover, E.W.N. Double unresolved approximations to multiparton scattering amplitudes. *Nucl. Phys. B* **1998**, *527*, 264–288.
40. Gehrmann-De Ridder, A.; Gehrmann, T.; Glover, E.W.N. Antenna subtraction at NNLO. *JHEP* **2005**, *9*, 56. [CrossRef]
41. Daleo, A.; Gehrmann, T.; Maitre, D. Antenna subtraction with hadronic initial states. *JHEP* **2007**, *4*, 16. [CrossRef]
42. Nigel Glover, E.W.; Pires, J. Antenna subtraction for gluon scattering at NNLO. *JHEP* **2010**, *6*, 96. [CrossRef]
43. Currie, J.; Glover, E.W.N.; Wells, S. Infrared Structure at NNLO Using Antenna Subtraction. *JHEP* **2013**, *4*, 66.
44. Currie, J.; Gehrmann, T.; Glover, E.W.N.; Huss, A.; Niehues, J.; Vogt, A. N^{3}LO corrections to jet production in deep inelastic scattering using the Projection-to-Born method. *JHEP* **2018**, *5*, 209.
45. Gehrmann, T.; Huss, A.; Niehues, J.; Vogt, A.; Walker, D.M. Jet production in charged-current deep-inelastic scattering to third order in QCD. *Phys. Lett. B* **2019**, *792*, 182–186.
46. Somogyi, G.; Trocsanyi, Z.; Del Duca, V. A Subtraction scheme for computing QCD jet cross sections at NNLO: Regularization of doubly-real emissions. *JHEP* **2007**, *1*, 70.
47. Somogyi, G.; Trocsanyi, Z. A Subtraction scheme for computing QCD jet cross sections at NNLO: Regularization of real-virtual emission. *JHEP* **2007**, *1*, 52.
48. Czakon, M. A novel subtraction scheme for double-real radiation at NNLO. *Phys. Lett.* **2010**, *B693*, 259–268. [CrossRef]
49. Czakon, M. Double-real radiation in hadronic top quark pair production as a proof of a certain concept. *Nucl. Phys. B* **2011**, *849*, 250–295.
50. Boughezal, R.; Melnikov, K.; Petriello, F. A subtraction scheme for NNLO computations. *Phys. Rev. D* **2012**, *85*, 034025.
51. Boughezal, R.; Liu, X.; Petriello, F. *N*-jettiness soft function at next-to-next-to-leading order. *Phys. Rev. D* **2015**, *91*, 094035.
52. Gaunt, J.; Stahlhofen, M.; Tackmann, F.J.; Walsh, J.R. N-jettiness Subtractions for NNLO QCD Calculations. *JHEP* **2015**, *9*, 58.
53. Magnea, L.; Maina, E.; Pelliccioli, G.; Signorile-Signorile, C.; Torrielli, P.; Uccirati, S. Local analytic sector subtraction at NNLO. *JHEP* **2018**, *12*, 107, Erratum in *JHEP* **2019**, *6*, 13. [CrossRef]
54. Magnea, L.; Pelliccioli, G.; Signorile-Signorile, C.; Torrielli, P.; Uccirati, S. Analytic integration of soft and collinear radiation in factorised QCD cross sections at NNLO. *JHEP* **2021**, *2*, 37.
55. Heinrich, G. Collider Physics at the Precision Frontier. *Phys. Rept.* **2021**, *922*, 1–69.
56. Kreimer, D.; Yeats, K. Algebraic Interplay between Renormalization and Monodromy. *arXiv* **2021**, arXiv:2105.05948.
57. Borinsky, M.; Capatti, Z.; Laenen, E.; Salas-Bernárdez, A. Flow-oriented perturbation theory. *arXiv* **2022**, arXiv:2210.05532.
58. Catani, S.; Gleisberg, T.; Krauss, F.; Rodrigo, G.; Winter, J.C. From loops to trees by-passing Feynman's theorem. *JHEP* **2008**, *9*, 65.
59. Buchta, S.; Chachamis, G.; Draggiotis, P.; Malamos, I.; Rodrigo, G. On the singular behaviour of scattering amplitudes in quantum field theory. *JHEP* **2014**, *11*, 14.
60. Tomboulis, E. Causality and Unitarity via the Tree-Loop Duality Relation. *JHEP* **2017**, *5*, 148. [CrossRef
61. Runkel, R.; Szőr, Z.; Vesga, J.P.; Weinzierl, S. Causality and loop-tree duality at higher loops. *Phys. Rev. Lett.* **2019**, *122*, 111603. Erratum in *Phys. Rev. Lett.* **2019**, *123*, 059902. [CrossRef] [PubMed]
62. Capatti, Z.; Hirschi, V.; Kermanschah, D.; Ruijl, B. Loop-Tree Duality for Multiloop Numerical Integration. *Phys. Rev. Lett.* **2019**, *123*, 151602.
63. Aguilera-Verdugo, J.J.; Driencourt-Mangin, F.; Hernandez Pinto, R.J.; Plenter, J.; Ramirez-Uribe, S.; Renteria Olivo, A.E.; Rodrigo, G.; Sborlini, G.F.; Torres Bobadilla, W.J.; Tracz, S. Open loop amplitudes and causality to all orders and powers from the loop-tree duality. *Phys. Rev. Lett.* **2020**, *124*, 211602.
64. Aguilera-Verdugo, J.d.J.; Driencourt-Mangin, F.; Hernández-Pinto, R.J.; Plenter, J.; Prisco, R.M.; Ramírez-Uribe, N.S.; Rentería-Olivo, A.E.; Rodrigo, G.; Sborlini, G.; Torres Bobadilla, W.J.; et al. A Stroll through the Loop-Tree Duality. *Symmetry* **2021**, *13*, 1029. [CrossRef]
65. Kromin, S.; Schwanemann, N.; Weinzierl, S. Amplitudes within causal loop-tree duality. *Phys. Rev. D* **2022**, *106*, 076006.
66. Capatti, Z.; Hirschi, V.; Pelloni, A.; Ruijl, B. Local Unitarity: A representation of differential cross-sections that is locally free of infrared singularities at any order. *JHEP* **2021**, *4*, 104.
67. Berghoff, M. Schwinger, ltd: Loop-tree duality in the parametric representation. *JHEP* **2022**, *10*, 178. [CrossRef]
68. Runkel, R.; Szőr, Z.; Vesga, J.P.; Weinzierl, S. Integrands of loop amplitudes within loop-tree duality. *Phys. Rev. D* **2020**, *101*, 116014.
69. Buchta, S.; Chachamis, G.; Draggiotis, P.; Rodrigo, G. Numerical implementation of the loop–tree duality method. *Eur. Phys. J.* **2017**, *C77*, 274.
70. Buchta, S. Theoretical foundations and applications of the Loop-Tree Duality in Quantum Field Theories. Ph.D Thesis, Universidad de Valencia, Valencia, Spain, 2015. arXiv:1509.07167.

71. Driencourt-Mangin, F.; Rodrigo, G.; Sborlini, G.F.R.; Torres Bobadilla, W.J. Interplay between the loop-tree duality and helicity amplitudes. *Phys. Rev. D* **2022**, *105*, 016012.
72. Capatti, Z.; Hirschi, V.; Kermanschah, D.; Pelloni, A.; Ruijl, B. Numerical Loop-Tree Duality: Contour deformation and subtraction. *JHEP* **2020**, *4*, 96.
73. Kermanschah, D. Numerical integration of loop integrals through local cancellation of threshold singularities. *JHEP* **2022**, *1*, 151.
74. Driencourt-Mangin, F.; Rodrigo, G.; Sborlini, G.F. Universal dual amplitudes and asymptotic expansions for $gg \to H$ and $H \to \gamma\gamma$ in four dimensions. *Eur. Phys. J. C* **2018**, *78*, 231.
75. Plenter, J. Asymptotic Expansions Through the Loop-Tree Duality. *Acta Phys. Polon. B* **2019**, *50*, 1983–1992. . 10.5506/APhysPolB.50.1983. [CrossRef]
76. Plenter, J.; Rodrigo, G. Asymptotic expansions through the loop-tree duality. *Eur. Phys. J. C* **2021**, *81*, 320. [CrossRef]
77. Plenter, J. Asymptotic Expansions and Causal Representations through the Loop-Tree Duality. Ph.D Thesis, Universidad de Valencia, Valencia, Spain, 2022.
78. Driencourt-Mangin, F.; Rodrigo, G.; Sborlini, G.F.R.; Torres Bobadilla, W.J. Universal four-dimensional representation of $H \to \gamma\gamma$ at two loops through the Loop-Tree Duality. *JHEP* **2019**, *2*, 143.
79. Driencourt-Mangin, F. Four-dimensional representation of scattering amplitudes and physical observables through the application of the Loop-Tree Duality theorem. PhD Thesis, Universidad de Valencia, Valencia, Spain, 2019. arXiv:1907.12450.
80. Aguilera-Verdugo, J.J.; Driencourt-Mangin, F.; Plenter, J.; Ramírez-Uribe, S.; Rodrigo, G.; Sborlini, G.F.; Torres Bobadilla, W.J.; Tracz, S. Causality, unitarity thresholds, anomalous thresholds and infrared singularities from the loop-tree duality at higher orders. *JHEP* **2019**, *12*, 163.
81. Hernandez-Pinto, R.J.; Sborlini, G.F.R.; Rodrigo, G. Towards gauge theories in four dimensions. *JHEP* **2016**, *2*, 44.
82. Sborlini, G.F.R.; Driencourt-Mangin, F.; Hernandez-Pinto, R.; Rodrigo, G. Four-dimensional unsubtraction from the loop-tree duality. *JHEP* **2016**, *8*, 160.
83. Sborlini, G.F.R.; Driencourt-Mangin, F.; Rodrigo, G. Four-dimensional unsubtraction with massive particles. *JHEP* **2016**, *10*, 162.
84. Ramírez-Uribe, S.; Hernández-Pinto, R.J.; Rodrigo, G.; Sborlini, G.F.R.; Torres Bobadilla, W.J. Universal opening of four-loop scattering amplitudes to trees. *JHEP* **2021**, *4*, 129.
85. Jesús Aguilera-Verdugo, J.; Hernández-Pinto, R.J.; Rodrigo, G.; Sborlini, G.F.R.; Torres Bobadilla, W.J. Mathematical properties of nested residues and their application to multi-loop scattering amplitudes. *JHEP* **2021**, *2*, 112.
86. Aguilera-Verdugo, J.J.; Hernandez-Pinto, R.J.; Rodrigo, G.; Sborlini, G.F.R.; Torres Bobadilla, W.J. Causal representation of multi-loop Feynman integrands within the loop-tree duality. *JHEP* **2021**, *1*, 69.
87. Bobadilla, W.J.T. Lotty – The loop-tree duality automation. *Eur. Phys. J. C* **2021**, *81*, 514.
88. Sborlini, G.F.R. Geometrical approach to causality in multiloop amplitudes. *Phys. Rev. D* **2021**, *104*, 036014. [CrossRef]
89. Torres Bobadilla, W.J. Loop-tree duality from vertices and edges. *JHEP* **2021**, *4*, 183.
90. Capatti, Z.; Hirschi, V.; Kermanschah, D.; Pelloni, A.; Ruijl, B. Manifestly Causal Loop-Tree Duality. *arXiv* **2020**, arXiv:2009.05509.
91. Chetyrkin, K.G.; Misiak, M.; Munz, M. Beta functions and anomalous dimensions up to three loops. *Nucl. Phys. B* **1998**, *518*, 473–494.
92. Luthe, T.; Maier, A.; Marquard, P.; Schröder, Y. Towards the five-loop Beta function for a general gauge group. *JHEP* **2016**, *7*, 127.
93. Baikov, P.A.; Chetyrkin, K.G.; Kühn, J.H. Five-Loop Running of the QCD coupling constant. *Phys. Rev. Lett.* **2017**, *118*, 082002.
94. Herzog, F.; Ruijl, B.; Ueda, T.; Vermaseren, J.A.M.; Vogt, A. The five-loop beta function of Yang-Mills theory with fermions. *JHEP* **2017**, *2*, 90.
95. Herzog, F. Zimmermann's forest formula, infrared divergences and the QCD beta function. *Nucl. Phys. B* **2018**, *926*, 370–380.
96. Bollini, C.G.; Giambiagi, J.J. Dimensional Renormalization: The Number of Dimensions as a Regularizing Parameter. *Nuovo Cim.* **1972**, *B12*, 20–26. [CrossRef]
97. 't Hooft, G.; Veltman, M.J.G. Regularization and Renormalization of Gauge Fields. *Nucl. Phys.* **1972**, *B44*, 189–213. [CrossRef]
98. Cicuta, G.M.; Montaldi, E. Analytic renormalization via continuous space dimension. *Lett. Nuovo Cim.* **1972**, *4*, 329–332. [CrossRef]
99. Ashmore, J.F. A Method of Gauge Invariant Regularization. *Lett. Nuovo Cim.* **1972**, *4*, 289–290. [CrossRef]
100. Capatti, Z.; Hirschi, V.; Ruijl, B. Local unitarity: Cutting raised propagators and localising renormalisation. *JHEP* **2022**, *10*, 120.